

Towards model based control of the Vertical Gradient Freeze crystal growth process

S. Ecklebe^{a,*}, F. Woittennek^b, J. Winkler^a, Ch. Frank-Rotsch^c, N. Dropka^c

^a*Institute of Control Theory, Technische Universität Dresden, 01062 Dresden, Germany*

^b*IACE, Private University for Health Sciences, Medical Informatics and Technology (UMIT), Eduard-Wallnoefer-Zentrum 1, A-6060 Hall in Tirol, Austria*

^c*Leibniz Institute for Crystal Growth (IKZ), Max-Born-Str. 2, 12489 Berlin, Germany*

Abstract

In this contribution tracking control designs using output feedback are presented for a two-phase Stefan problem arising in the modeling of the Vertical Gradient Freeze process. The two-phase Stefan problem, consisting of two coupled free boundary problems, is a vital part of many crystal growth processes due to the temporally varying extent of the solid and liquid domains during growth. After discussing the special needs of the process, collocated as well as flatness-based state feedback designs are carried out. To render the setup complete, an observer design is performed, using a flatness-based approximation of the original distributed parameter system (DPS). The quality of the provided approximations as well as the performance of the open and closed loop control setups is analysed in several simulations.

Keywords: Vertical Gradient Freeze, Industrial Crystallization, Distributed Parameter Systems, Differential Flatness, Observer Design

1. Introduction

The Vertical Gradient Freeze (VGF) process is the most important technology for the production of bulk compound semiconductor crystals like Gallium-Arsenide (GaAs) or Indium-Phosphide (InP) [1] which are especially used for manufacturing high-power and high-frequency electronics as well as infrared light-emitting and laser diodes. For these purposes the crystals have to meet high requirements with respect to their purity and structural perfection.

The basic VGF setup is shown in Figure 1: A crucible, usually made of boron nitride and holding the material which is to be molten and then solidified, is surrounded by several heaters. The whole setup is enclosed by a thick insulation. At the bottom of the crucible a seed crystal is placed which defines the orientation of the crystal to be grown. After melting up the material in the crucible (without destroying the seed crystal) the temperature field has to be adjusted and tracked by means of the heat input of the heaters in such a way that the melt solidifies from the bottom to the top in a desired manner. This means that a) the solid-liquid-interface (phase boundary) maintains a plain shape and b) the growth rate (i.e., the velocity of the solid-liquid-interface) and the temperature gradient at the phase boundary are kept on a certain level throughout the whole process as they have been identified as crucial factors regarding the quality of the grown crystal (see eg. [2] for an analysis regarding the related Czochralski process). This solidification by using a travelling vertical temperature gradient is where the name of the process originates

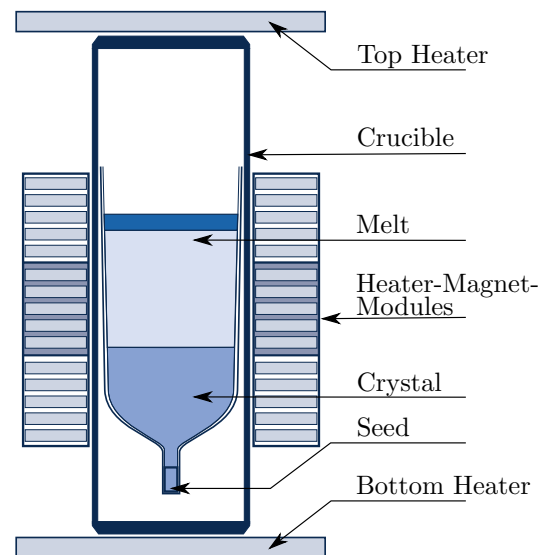


Figure 1: Sketch of a VGF crystal growth furnace.

*Corresponding author: stefan.ecklebe@tu-dresden.de

from. To affect the process, a top and a bottom heater in form of plane disks, as well as three jacket heaters in form of coils are mounted in the plant.

Due to its importance the improvement of this process is in focus of the scientific community, resulting e.g. in the application of external travelling magnetic fields (TMFs) [3, 4, 5, 6]. However, a topic that has not received much attention is the process control of this growth technique. This lack of coverage has two main reasons: Firstly, in-situ measurements from the growing crystal (e.g. the shape and position of the phase boundary or the growth rate) as a prerequisite for feedback control are not available or not applicable in an industrial environment [7]. Secondly, the coupled free boundary problems for crystal and melt form a so called two-phase Stefan problem (SP) [8] which is of nonlinear nature.

As is well known, the first issue can be tackled by an appropriate observer design which has already been presented in [9] for the one-phase SP. However, regarding the implementation a simulation model is needed for the observer. Since the simulation of solidification processes and therefore of free boundary problems (FBPs) has been under investigation over the last decades, there are a lot of different numerical schemes like the Enthalpy[10], Level-Set[11] or Moving-Grid[12] method available, to name just a few. However, being numerical schemes, identifying their variables with a state-space representation for subsequent observer design is not straight forward.

The second issue is broadly discussed in the framework of DPSs. Making the assumption, that the temperature distribution in one phase is constant (which is often justified due to its dominant spatial extent) yields the so called one-phase SP. Regarding this special case, results are lately available for the feedforward design [13] using flatness-, as well as for feedback designs using enthalpy-[14, 15], geometrically- [16] or backstepping- [17] based approaches. Regarding the full problem, [18] extends the flatness-based motion planning to the two-phase SP, while [19] addresses the problem from the side of optimal control. Concerning feedback, a direct extension of the approaches for the one-phase case is not feasible since for the two-phase case, the coupling between the two FBPs has to be taken into account. In this context it is noteworthy that [20] already states a Lyapunov-based control law for the two-phase SP with actuation at one boundary. However, according to our current knowledge there are no results available for the tracking control of the two-phase SP via output feedback concerning multiple inputs.

1.1. Objective and structure of the paper

The main goal of this contribution is to introduce methods for tracking control of a one dimensional, two-phase SP via output feedback (resp. observer based state feedback) as a starting point for an improvement of process control in the VGF growth process.

To reach this goal, the paper is structured as follows: In Section 2 the distributed parameter model of the pro-

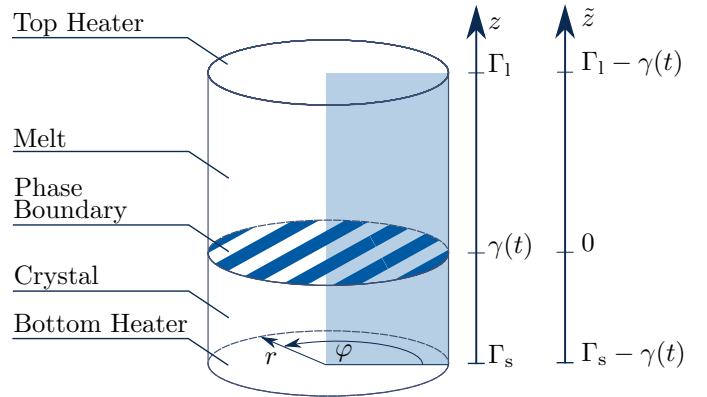


Figure 2: Schematics of the cylindrical coordinate system (r, φ, z, t) , a meridional plane (blue) and the shifted coordinate $\tilde{z} = z - \gamma(t)$.

cess is introduced. Section 3 outlines a feedforward control design which is based on the flat parametrisation of the solution by means of power series. This feedforward subsequently serves as the source of a reference temperature profile. Based on this, Section 4 introduces a collocated controller that tracks this reference by utilizing state feedback. Looking at the problem from another point of view and further exploiting the flatness property, Section 5 presents a flatness based state feedback control. This approach relies on a finite dimensional approximation of the system dynamics which is obtained from the parametrisation in Section 3. To comply with the specific demands of the process, different variants of both control concepts are introduced. Since all designs depend on state measurements to some extent, in Section 6 a lumped observer for the flat system approximation is shown. Section 7 presents simulation results for the different control setups using state and output feedback. Finally, a summary and an outlook to further work is given.

2. Modelling of the VGF process

In this section a one dimensional distributed parameter model of the VGF process plant is derived. For this purpose, the following simplifications are made: The crucible geometry is approximated by a cylinder. Thus, the distribution of the system temperature T in the crucible depends on the time t and the cylindrical coordinates, given by radius r , angle φ and height z , as depicted in Figure 2. Furthermore, any convective effects in the melt are neglected. This is reasonable due to the dominating heat transport by diffusion. Beyond, making use of the fact that the plant itself is rotationally symmetric to the longitudinal axis, the model can be reduced to a meridional plane of the crucible by taking the average over the angular coordinate φ . In addition, the lateral heaters are assumed to be used as active isolation, avoiding any heat loss in radial direction and therefore rendering the phase boundary a horizontal line. Hence, averaging over the radius r allows further reduction of the domain to a line whose

boundaries represent the bottom and top of the crucible at $z = \Gamma_s$ and $z = \Gamma_l$, respectively. Summarising, the system temperature is given by $T(z, t)$ for $\Gamma_s \leq z \leq \Gamma_l$ and $t > 0$ while the phase boundary is given by $\gamma(t) \in (\Gamma_s, \Gamma_l)$.

This leads to the one dimensional nonlinear heat equation [21]

$$\frac{\partial}{\partial t} \left(\rho(T(z, t)) c_p(T(z, t)) T(z, t) \right) = \frac{\partial}{\partial z} \left(k(T(z, t)) \frac{\partial}{\partial z} T(z, t) \right), \quad z \in (\Gamma_s, \Gamma_l) \setminus \{\gamma(t)\} \quad (1)$$

with the density ρ , the specific heat capacity c_p and k the thermal conductivity being temperature-dependent. Assuming piecewise constant parameters for the solid and the liquid phase it is possible to decompose the nonlinear system (1) into two FBPs for the temperatures $T_s(z, t)$ and $T_l(z, t)$:

$$\partial_t T_s(z, t) = \alpha_s \partial_z^2 T_s(z, t), \quad z \in \Omega_s = (\Gamma_s, \gamma(t)) \quad (2a)$$

$$k_s \partial_z T_s(\Gamma_s, t) = \delta_s u_s(t) \quad (2b)$$

$$T_s(\gamma(t), t) = T_m \quad (2c)$$

$$\partial_t T_l(z, t) = \alpha_l \partial_z^2 T_l(z, t), \quad z \in \Omega_l = (\gamma(t), \Gamma_l) \quad (2d)$$

$$k_l \partial_z T_l(\Gamma_l, t) = \delta_l u_l(t) \quad (2e)$$

$$T_l(\gamma(t), t) = T_m. \quad (2f)$$

Herein, the index ‘‘s’’ denotes the solid and the index ‘‘l’’ the liquid phase. The heat flows $u_s(t)$ and $u_l(t)$ at the bottom and the top boundary are considered as system inputs with the orientation factors $\delta_s = -1$ and $\delta_l = 1$. The partial derivative of the quantity $T(z, t)$ with respect to z or t is denoted by $\partial_z T(z, t)$ or $\partial_t T(z, t)$. Finally, $\alpha_s = \frac{k_s}{\rho_s c_{p,s}}$ and $\alpha_l = \frac{k_l}{\rho_l c_{p,l}}$ denote the thermal diffusivities.

Due to the moving phase boundary latent heat is released by the solidification process. This effect can be modelled by the Stefan condition [22]

$$\rho_m L \dot{\gamma}(t) = k_s \partial_z T_s(\gamma(t), t) - k_l \partial_z T_l(\gamma(t), t) \quad (3)$$

with the density of the melt at melting temperature ρ_m and the specific latent heat L .

Together, the equations (2) and (3) form the two-phase SP whose state is given by

$$\mathbf{x}(\cdot, t) = \begin{pmatrix} T(\cdot, t) \\ \gamma(t) \end{pmatrix} \in X = L_2(\Omega) \times (\Gamma_s, \Gamma_l) \quad (4)$$

with $\Omega = [\Gamma_s, \Gamma_l]$. Note that the PDE-ODE system defined by (2) and (3) is inherently nonlinear since the domains of (2b) and (2e) depend on the state variable $\gamma(t)$. Furthermore, with the system boundaries admitting access for measurements, the system output is given by

$$\boldsymbol{\eta}(t) = \mathbf{h}(\mathbf{x}(t)) = \begin{pmatrix} T(\Gamma_s, t) \\ T(\Gamma_l, t) \end{pmatrix}. \quad (5)$$

Exploiting the identical structure of the diffusion equations, the following sections will – where applicable – resort to discuss merely one generic temperature distribution $T_\circ(z, t)$ for $z \in \Omega_\circ$ with \circ to be replaced by the indices s or l depending on the considered domain.

3. Feedforward control

This section gives a short recap of a feedforward control design which was presented in [13] for the one-phase and in [23] for the two-phase case to which the reader is kindly directed for further details.

To eliminate the temporal dependency in the boundary conditions of (2), the coordinate transform

$$\tilde{T}_\circ(\tilde{z}, t) = T_\circ(z, t) \quad \text{with} \quad \tilde{z} := z - \gamma(t) \quad (6)$$

is introduced. As a consequence the phase boundary is shifted into the origin of a new, moving reference frame as it can be seen on the right-hand side of Figure 2. The resulting¹ system is given by

$$\partial_t \tilde{T}_\circ(\tilde{z}, t) = \alpha_\circ \partial_{\tilde{z}}^2 \tilde{T}_\circ(\tilde{z}, t) + \dot{\gamma}(t) \partial_{\tilde{z}} \tilde{T}_\circ(\tilde{z}, t) \quad (7a)$$

$$k_\circ \partial_{\tilde{z}} \tilde{T}_\circ(\tilde{\Gamma}_\circ(t), t) = \delta_\circ u_\circ(t) \quad (7b)$$

$$\tilde{T}_\circ(0, t) = T_m \quad (7c)$$

$$\dot{\gamma}(t) = \frac{1}{L \rho_m} \left(k_s \partial_{\tilde{z}} \tilde{T}_s(0, t) - k_l \partial_{\tilde{z}} \tilde{T}_l(0, t) \right) \quad (7d)$$

where $\tilde{\Gamma}_\circ(t) := \Gamma_\circ - \gamma(t)$.

By expressing the solution $\tilde{T}_\circ(\tilde{z}, t)$ of (7) in terms of a power series in \tilde{z} :

$$\tilde{T}_\circ(\tilde{z}, t) = \sum_{i=0}^{\infty} c_{\circ,i}(t) \frac{\tilde{z}^i}{i!}, \quad (8)$$

plugging it into (7a) and comparing the coefficients of like powers of \tilde{z} the recursion formula

$$c_{\circ,i+2}(t) = \frac{1}{\alpha_\circ} \left(\partial_t c_{\circ,i}(t) - \dot{\gamma}(t) c_{\circ,i+1}(t) \right) \quad i = 0, \dots, \infty \quad (9)$$

is obtained. A closer examination of (8) shows that the following holds for the initial coefficients :

$$c_{\circ,0}(t) = \tilde{T}_\circ(0, t) = T_m, \quad c_{\circ,1}(t) = \partial_{\tilde{z}} \tilde{T}_\circ(0, t). \quad (10)$$

By utilizing the Stefan condition (7d) solved for the gradient at the liquid side

$$\partial_{\tilde{z}} \tilde{T}_l(0, t) = \frac{1}{k_l} \left(k_s \partial_{\tilde{z}} \tilde{T}_s(0, t) - \rho_m L \dot{\gamma}(t) \right) \quad (11)$$

it follows that the solution for both phases can be expressed by the gradient in the solid $\partial_{\tilde{z}} \tilde{T}_s(0, t)$ and the growth rate $\dot{\gamma}(t)$. Thus, the system (2) is differentially flat with a flat output

$$\mathbf{y}(t) = \begin{pmatrix} y_1(t) \\ y_2(t) \end{pmatrix} = \begin{pmatrix} \partial_{\tilde{z}} \tilde{T}_s(0, t) \\ \gamma(t) \end{pmatrix}. \quad (12)$$

Assuming convergence and truncating the series (8) at an order N , the mapping

$$\tilde{\mathbf{T}}^N(\tilde{z}, t) = \begin{pmatrix} \tilde{T}_s^N(\tilde{z}, t) \\ \tilde{T}_l^N(\tilde{z}, t) \end{pmatrix} = \boldsymbol{\Theta}^N \left(\partial_{\tilde{z}} \tilde{T}_s(0, t), \dots, \partial_{\tilde{z}} \tilde{T}_s^{(\alpha_1)}(0, t), \right. \\ \left. \gamma(t), \dots, \gamma^{(\alpha_2)}(t) \right) \quad (13)$$

¹For details see Appendix A.1.

where $\alpha_1 = \lfloor N/2 \rfloor - 1$ and $\alpha_2 = \lfloor N/2 \rfloor$ can be formulated. Finally, choosing the trajectories for the components of $\mathbf{y}(t)$ as

$$y(t) = y_A + (y_B - y_A)\phi\left(\frac{t}{\vartheta}\right) \quad (14)$$

where

$$\phi(\tau) = \frac{1}{2} \left(1 + \tanh\left(\frac{2(2\tau - 1)}{(4\tau(1 - \tau))^\sigma}\right) \right) \quad (15)$$

is of Gevrey-order $\alpha_G = 1 + \frac{1}{\sigma}$ [24] convergence of the scheme can be shown for $\alpha_G \leq 2$ [18].

Hence, by utilizing the boundary condition (7b) the inputs $u_s(t)$ and $u_l(t)$ are obtained by evaluating the temperature profile which is given the mapping (13). This yields the input map

$$\mathbf{u}(t) = \Phi^N(y_1(t), \dots, y_1^{(\alpha_1)}(t), y_2(t), \dots, y_2^{(\alpha_2)}(t)) \quad (16)$$

given in terms of the flat output.

Summarising, by prescribing reference trajectories $\mathbf{y}_r(t)$ for the flat output $\mathbf{y}(t)$, a reference temperature distribution $T_r(z, t)$ and input $\mathbf{u}_r(t)$ can be computed. These results will serve as the basis for the control design in the next section.

4. Collocated feedback

This section will present an approach for the collocated tracking control of the two-phase SP. To do this, different control errors are compared concerning their suitability concerning the VGF process and the stability of the closed loop is investigated. In detail, the profile $T_r(z, t)$, introduced in the previous section, will be utilised as control reference while the input trajectories $\mathbf{u}_r(t)$ are not needed. Note that all considerations in this section are conducted in the original spatially fixed coordinates.

4.1. Error definitions

Choosing the distributed temperature error

$$e(z, t) := T(z, t) - T_r(z, t) \quad (17)$$

as deviation of the system temperature $T(z, t)$ from the reference profile $T_r(z, t)$ over the complete spatial domain as in [20] seems natural at a first glance. However, this is not useful in order to meet the technological requirements: Due to the biphasic character of the system, convergence of $e(z, t)$ into the origin implies convergence of the phase boundary position error

$$\Delta\gamma(t) = \gamma(t) - \gamma_r(t). \quad (18)$$

However, the quality of the crystal does not depend on the position of the phase boundary but rather on its velocity. Moreover, it seems more natural to compare the temperature of like phases only. As a consequence the error is defined on the basis of a shifted reference trajectory

$$\tilde{e}(z, t) := T(z, t) - T_r(z - \Delta\gamma(t), t) \quad (19)$$

in combination with (18). To do so, however, the planning for the reference profile $T_r(z, t)$ has to be carried out on an extended spatial domain. More precisely, for any admissible $\Delta\gamma(t)$, the profile $T_r(z - \Delta\gamma(t), t)$ must not be evaluated outside of its domain. Considering the plant properties, it follows that $\Delta\gamma(t) \in (\Gamma_s - \Gamma_l, \Gamma_l - \Gamma_s)$. Therefore, a feasible domain for $T_r(z, t)$ would be $(z, t) \in \Omega_r \times \mathbb{R}_+$, with $\Omega_r = [2\Gamma_s - \Gamma_l, 2\Gamma_l - \Gamma_s]$. Analysing² (19), the phase dependent tracking error $\tilde{e}_o(z, t) = T_o(z, t) - T_{o,r}(z - \Delta\gamma(t), t)$ is governed by

$$\begin{aligned} \partial_t \tilde{e}_o(z, t) &= \alpha_o \partial_z^2 \tilde{e}_o(z, t) + \Delta\dot{\gamma}(t) \partial_z T_{o,r}(z - \Delta\gamma(t), t) \\ z &\in \Omega_o \end{aligned} \quad (20a)$$

$$\partial_z \tilde{e}_o(\Gamma_o, t) = \frac{\delta_o}{k_o} u(t) - \partial_z T_{o,r}(\Gamma_o - \Delta\gamma(t), t) \quad (20b)$$

$$\tilde{e}_o(\gamma(t), t) = 0 \quad (20c)$$

$$\Delta\dot{\gamma}(t) = \frac{1}{L\rho_m} (k_s \tilde{e}_s(\gamma(t), t) - k_l \tilde{e}_l(\gamma(t), t)). \quad (20d)$$

Herein, the second term in the righthand side of (20b) can be understood as a feedforward part. However, it does not coincide with the reference input $\mathbf{u}_r(t)$ due to the spatial shift. Finally, the error state is given by

$$\boldsymbol{\xi}(z, t) = \begin{pmatrix} \tilde{e}_o(z, t) \\ \Delta\gamma(t) \end{pmatrix} \in X. \quad (21)$$

4.2. Control law

A very intuitive way to manipulate the system is to convert (20b) into

$$\partial_z \tilde{e}_o(\Gamma_o, t) = -\delta_o \kappa_o \tilde{e}_o(\Gamma_o, t). \quad (22)$$

This leads to the feedback law

$$u_o(t) = \frac{k_o}{\delta_o} \partial_z T_{o,r}(z - \Delta\gamma(t), t) - \kappa_o k_o \tilde{e}_o(\Gamma_o, t). \quad (23)$$

Albeit reasonable in its composition, the control law only honours the boundary error at $z = \Gamma_o$. Hence, further analysis is required to ensure convergence of $\Delta\dot{\gamma}(t)$.

4.3. Stability analysis

Although the framework which will be applied here was already laid out in [25] for finite dimensional systems, the nomenclature, used in the following is borrowed from [26] due to its application for the infinite dimensional case. Keeping in mind that the tracking of the growth velocity $\dot{\gamma}(t)$ is more important than the exact adjustment of the boundary position $\gamma(t)$, it is apparent that to obtain the desired results, $\boldsymbol{\xi}(z, t)$ may not necessarily converge into the origin but rather into a compact subset of the state space, given by

$$\mathcal{A} := \{(\boldsymbol{\xi}, \gamma)^T \in X \mid \boldsymbol{\xi} = 0\} \quad (24)$$

²Details in Appendix A.2.

with X from (4). Assuming that $\boldsymbol{\xi}(z, t) \in \mathcal{A}$ for some t , (20d) yields that $\Delta\dot{\gamma}(t) = 0$. Using this information, (20a) gives $\partial_t \tilde{e}(z, t) = 0$. Thus $\boldsymbol{\xi}(z, 0) \in \mathcal{A} \implies \boldsymbol{\xi}(z, t) \in \mathcal{A} \quad \forall t \geq 0$, rendering \mathcal{A} an invariant set of the system (20). Furthermore let the distance of an element $\boldsymbol{x} \in X$ to \mathcal{A} be given by $|\boldsymbol{x}|_{\mathcal{A}} := \min \{ \|\boldsymbol{x} - \boldsymbol{y}\|_X \mid \boldsymbol{y} \in \mathcal{A} \}$ and consider the function classes:

$$\mathcal{K} := \{ f : \mathbb{R}_+ \mapsto \mathbb{R}_+ \mid f(0) = 0, f \text{ is continuous and strictly increasing} \}$$

$$\mathcal{K}_\infty := \{ f \in \mathcal{K} \mid f \text{ is unbounded} \} .$$

As stated in [26], if there exists a Lyapunov function $V(\boldsymbol{\xi})^3$, so that

$$a_1(|\boldsymbol{\xi}|_{\mathcal{A}}) \leq V(\boldsymbol{\xi}) \leq a_2(|\boldsymbol{\xi}|_{\mathcal{A}}) \quad \forall \boldsymbol{\xi} \in X \quad (25a)$$

$$\dot{V}(\boldsymbol{\xi}) \leq -b(|\boldsymbol{\xi}|_{\mathcal{A}}) \quad \forall \boldsymbol{\xi} \in X \quad (25b)$$

with $a_1, a_2 \in \mathcal{K}_\infty$ and $b \in \mathcal{K}$ hold, the system (20) is uniformly globally asymptotically stable with respect to \mathcal{A} . For this purpose, the Lyapunov function candidate

$$V(\boldsymbol{\xi}) = \frac{1}{2} \int_{\Gamma_s}^{\Gamma_1} \tilde{e}^2(z, t) dz \quad (26)$$

is used, which fulfils condition (25a). Furthermore, in the first part of Appendix B it is shown that for a simplified reference profile $T_r(z, t)$, the candidate (26) satisfies (25b). Thus, rendering it a Lyapunov function for (20) with respect to \mathcal{A} . Softening those demands on $T_r(z, t)$ is possible but leads to stricter requirements for the phase boundary error $\Delta\gamma(t)$, which are again hard to show for the general case. The detailed steps are given in the second part of Appendix B. However, simulation results show that the system state $\boldsymbol{\xi}$ converges to \mathcal{A} for non-trivial reference profiles, too.

5. Distributed Feedback

Exploiting the fact that parametrisation of the system (2)-(3) which is introduced in Section 3 is differentially flat [13, 18] with the flat output (12), this property can be used to design a feedback in a straight-forward fashion without the explicit computation of a reference temperature profile.

5.1. System State

In [27, Ch. 5] a state space representation for a diffusion equation is given by means of the series coefficients of a power approximation. Therein, the components of a new state $\boldsymbol{\zeta}_o^N(t) := (c_{o,1}(t), \dots, c_{o,N}(t))^T$ belong to an approximation of an order N . Instead of extending this

³ For better readability, in the following the arguments of $\boldsymbol{\xi}(z, t)$ are omitted.

approach by combining the coefficients of the solid and liquid approximations into an extended state vector $\bar{\boldsymbol{\zeta}}^N(t) = (\boldsymbol{x}_s^{N^T}(t), \boldsymbol{x}_l^{N^T}(t))^T$ one may directly use the appropriate derivatives of the flat output. Hence, the state components $\chi_n^N(t)$, $1 \leq n \leq M$ with $M = (\alpha_1 + \alpha_2 + 2)$ in flat coordinates constitute the state vector $\boldsymbol{\chi}^N(t) \in \mathbb{R}^M$ which reads:

$$\boldsymbol{\chi}^N(t) = \left(y_1(t), \dots, y_1^{(\alpha_1)}(t), y_2(t), \dots, y_2^{(\alpha_2)}(t) \right)^T . \quad (27)$$

Herein, the required derivatives can be obtained from the iterated recursion formulas for both phases, cf. (9), for clarity condensed in the map

$$\boldsymbol{\chi}^N(t) = \boldsymbol{\psi}^N \left(\bar{\boldsymbol{\zeta}}^N(t) \right) . \quad (28)$$

Thus, examining the components of the derivative $\dot{\boldsymbol{\chi}}^N(t)$ two integrator chains become apparent:

$$\dot{\chi}_n^N(t) = \begin{cases} y_1^{(n)}(t) & \text{for } 1 \leq n \leq \alpha_1 + 1 \\ y_2^{(n - (\alpha_1 + 1))}(t) & \text{for } \alpha_1 + 1 < n \leq M . \end{cases} \quad (29)$$

Herein, the yet unknown derivatives $y_1^{(\alpha_1 + 1)}$ and $y_2^{(\alpha_2 + 1)}$ can be obtained from an extended version of (28) by using the extended coefficient state $\bar{\boldsymbol{\zeta}}^{N+1}(t)$:

$$\boldsymbol{\chi}^{N+1}(t) = \boldsymbol{\psi}^{N+1} \left(\bar{\boldsymbol{\zeta}}^{N+1}(t) \right) . \quad (30)$$

However this mapping requires the coefficients $c_{s,N+1}(t)$ and $c_{l,N+1}(t)$. Fortunately, these can be acquired from the respective boundary conditions of both phases, cf. (7b), after inserting the series expansion

$$c_{o,N+1}(t) = \frac{N!}{\Gamma_o^N} k_o \left(\delta_o u_o(t) - \sum_{i=0}^{N-1} c_{o,i+1}(t) \frac{\tilde{z}^i}{i!} \right) \quad (31)$$

wherein the coefficients $c_{o,1}(t)$ to $c_{o,N}(t)$ can readily be computed from $\boldsymbol{\chi}^N(t)$. According to (5), the outputs of each phase are given by

$$\eta_o(t) = \tilde{T}_o(\tilde{\Gamma}_o(t), t) = \sum_{i=0}^N c_{o,i}(t) \frac{\tilde{\Gamma}_o(t)^i}{i!} . \quad (32)$$

Hence, by using $\bar{\boldsymbol{\psi}}^N(\cdot)$, the inverse of the map (28), the output can be written as

$$\boldsymbol{\eta}_{\text{flat}}(t) = \boldsymbol{h}_{\text{flat}} \left(\bar{\boldsymbol{\psi}}^N \left(\boldsymbol{\chi}^N(t) \right) \right) . \quad (33)$$

5.2. Feedback Design

Regarding $y_1(t)$ and $y_2(t)$ as the outputs of the system, the tracking errors

$$\varepsilon_j(t) = y_j(t) - y_{j,r}(t), \quad j = 1, 2 \quad (34)$$

are defined. Hence, the decoupled linear error dynamics

$$\varepsilon_1^{(\alpha_1+1)}(t) = - \sum_{i=0}^{\alpha_1} \kappa_{1,i} \varepsilon_1^{(i)}(t) \quad (35a)$$

$$\varepsilon_2^{(\alpha_2+1)}(t) = - \sum_{i=0}^{\alpha_2} \kappa_{2,i} \varepsilon_2^{(i)}(t) \quad (35b)$$

are prescribed by choosing appropriate coefficients κ_1 and κ_2 . Defining the new inputs $v_1(t) := y_1^{(\alpha_1+1)}(t)$ and $v_2(t) := y_2^{(\alpha_2+1)}(t)$, by using the inverse of (30)

$$\bar{\zeta}^{N+1}(t) = \bar{\psi}^{N+1}(\chi^N(t), (v_1(t), v_2(t))^T), \quad (36)$$

the extended series coefficient set can be computed. Lastly, evaluation of (16) yields the control input $\mathbf{u}(t)$.

However, this design inherits the problem that an already grown crystal will be remelted if the measured interface position is ahead of the reference. Therefore, in view of the shifted error system (19), the pair $(y_1(t), \dot{y}_2(t))$ may be regarded as the output of a modified system, yielding $\tilde{\varepsilon}_2(t) = \dot{y}_2(t) - \dot{y}_{2,r}(t)$ as well as the dynamics

$$\tilde{\varepsilon}_2^{(\alpha_2)}(t) = - \sum_{i=0}^{\alpha_2-1} \tilde{\kappa}_{2,i} \tilde{\varepsilon}_2^{(i)}(t) \quad (37)$$

instead of (35b). Thus, a modified virtual input can be stated as $\tilde{v}_2(t) := \tilde{\varepsilon}_2^{(\alpha_2)}(t) + y_{2,r}^{(\alpha_2+1)}(t)$ which, by using (36) and (16) with $\tilde{v}_2(t)$ instead of $v_2(t)$, yields the modified control input $\tilde{\mathbf{u}}(t)$.

6. Observer Design

This section performs an observer design as shown in [28], however in this case based on the flat system state (27). The estimated system with the state $\hat{\mathbf{x}}(t)$ is given by the copy

$$\dot{\hat{\mathbf{x}}}(t) = \mathbf{f}(\hat{\mathbf{x}}(t), \mathbf{u}(t)) + \mathbf{L}(t)\bar{\boldsymbol{\eta}}(t) \quad (38a)$$

$$\hat{\boldsymbol{\eta}}(t) = \mathbf{h}(\hat{\mathbf{x}}(t)) \quad (38b)$$

with $\mathbf{L}(t)$ to be chosen later on and $\bar{\boldsymbol{\eta}}(t) = \hat{\boldsymbol{\eta}}(t) - \boldsymbol{\eta}(t)$. The plant model (38) is extended in the following way:

$$\dot{\mathbf{x}}(t) = \mathbf{f}(\mathbf{x}(t), \mathbf{u}(t) + \boldsymbol{\mu}(t)), \quad \boldsymbol{\eta}(t) = \mathbf{h}(\mathbf{x}(t) + \boldsymbol{\nu}(t)). \quad (39)$$

Herein, $\boldsymbol{\mu}(t)$ and $\boldsymbol{\nu}(t)$ represent disturbances acting on the system input and output, respectively. Furthermore, denoting $\bar{\mathbf{x}}(t) = \hat{\mathbf{x}}(t) - \mathbf{x}(t)$, the observer error dynamics

$$\dot{\bar{\mathbf{x}}}(t) = \mathbf{f}(\hat{\mathbf{x}}(t), \mathbf{u}(t)) + \mathbf{L}(t)\bar{\boldsymbol{\eta}}(t) - \mathbf{f}(\mathbf{x}(t), \mathbf{u}(t) + \boldsymbol{\mu}(t)) \quad (40a)$$

$$\bar{\boldsymbol{\eta}}(t) = \mathbf{h}(\hat{\mathbf{x}}(t)) - \mathbf{h}(\mathbf{x}(t) + \boldsymbol{\nu}(t)) \quad (40b)$$

is obtained. In the following, the computation of $\mathbf{L}(t)$ will be performed on a linearisation of (40) along the reference trajectory $\mathbf{y}_r(t)$, given by:

$$\dot{\hat{\mathbf{x}}}(t) = \mathbf{A}(t)\bar{\mathbf{x}}(t) - \mathbf{B}(t)\boldsymbol{\mu}(t) + \mathbf{L}(t)\bar{\boldsymbol{\eta}}(t) \quad (41a)$$

$$\bar{\boldsymbol{\eta}}(t) = \mathbf{C}(t)(\bar{\mathbf{x}}(t) - \boldsymbol{\nu}(t)). \quad (41b)$$

By defining the cost functional

$$J = \bar{\mathbf{x}}^T(0)\mathbf{S}\bar{\mathbf{x}}(0) + \int_0^t \boldsymbol{\mu}^T(t)\mathbf{R}\boldsymbol{\mu}(t) + \bar{\boldsymbol{\eta}}^T(t)\mathbf{Q}\bar{\boldsymbol{\eta}}(t) dt \quad (42)$$

where $\mathbf{S} \in \mathbb{R}^{M \times M}$ and $\mathbf{R}, \mathbf{Q} \in \mathbb{R}^{2 \times 2}$ denote penalties concerning the initial error as well as the disturbances on input and output, respectively. As [29, Th. 40, p.378] states, using the solution $\boldsymbol{\Pi}(t) \in \mathbb{R}^{M \times M}$ of the Filtering Riccati Differential Equation (FDRE)

$$\begin{aligned} \dot{\boldsymbol{\Pi}}(t) &= \boldsymbol{\Pi}(t)\mathbf{A}^T(t) + \mathbf{A}(t)\boldsymbol{\Pi}(t) \\ &\quad - \boldsymbol{\Pi}(t)\mathbf{C}^T(t)\mathbf{Q}\mathbf{C}(t)\boldsymbol{\Pi}(t) \\ &\quad + \mathbf{B}(t)\mathbf{R}^{-1}\mathbf{B}^T(t) \end{aligned} \quad (43a)$$

with the initial condition

$$\boldsymbol{\Pi}(0) = \mathbf{S}^{-1}, \quad (43b)$$

the choice

$$\mathbf{L}(t) := -\boldsymbol{\Pi}(t)\mathbf{C}^T(t)\mathbf{Q} \quad (44)$$

yields the optimal estimation for (41) regarding (42). Note that the solution of (43) can be done in advance.

7. Results

The theoretical results of the previous sections will now be evaluated by simulations. A finite element method (FEM) approximation using the boundary-immobilisation method will serve as a simulation model to compare the different feedback designs on a process oriented benchmark from the VGF process. The corresponding parameters are given in Table 1.

7.1. Setup and feedforward

For the trajectory planning, the following initial situation is assumed: The phase boundary is resting ($\dot{\gamma}(0) = 0 \text{ m s}^{-1}$) at $\gamma(0) = 0.2 \text{ m}$. Furthermore, as a result of a previous step (as shown in [18]) a gradient of $\partial_t T_s(\gamma(0), 0) = 17 \text{ K cm}^{-1}$ has been established at the solid side of the phase boundary. Now, the growth process is performed by prescribing $\gamma_r(t)$. Figure 3 shows the generated trajectories for $\partial_t T_{s,r}(\gamma_r(t), t)$ and $\gamma_r(t)$ as well as the calculated system inputs $u_s(t)$ and $u_l(t)$.

7.2. Feedback

To emulate a real growth process, an initial error of $\gamma_e(0) = 100 \text{ mm}$ and $\dot{\gamma}_e(0) = -3 \text{ mm h}^{-1}$ is introduced to the test-setup. To gain an extensive overview, two versions of the collocated controller from Section 4 are evaluated, one using the fixed error definition from (17) and one using the shifted error from (19). Furthermore, two variants

⁴The given unit refers to the second argument

Table 1: Parameters of the System

Name	Symbol	Value (s/l)	Unit
Spec. heat cap.	c_p	423.59 / 434	$\text{J kg}^{-1} \text{K}^{-1}$
Therm. conduct.	k	7.17 / 17.8	$\text{W m}^{-1} \text{K}^{-1}$
Therm. diffus.	α_s	$3.27 \cdot 10^{-6} /$	$\text{m}^2 \text{s}^{-1}$
	α_l	$7.19 \cdot 10^{-6}$	$\text{m}^2 \text{s}^{-1}$
Densities	ρ_s	5171.24 /	kg m^{-3}
	ρ_l	5702.37	kg m^{-3}
	ρ_m	5713.07	kg m^{-3}
Melting temp.	T_m	1511.15	K
Spec. latent heat	L	$668.5 \cdot 10^3$	J kg^{-1}
Left Boundary	Γ_s	0	m
Right Boundary	Γ_l	0.4	m
Feedf. Appr. Order	N_{ff}	10	
Obs. Approx. Order	N_{ob}	5	
Cont. Approx. Order	N_{fb}	5	
Imp. Weight Mat.	\mathbf{R}	$1 \cdot 10^{-4} \mathbf{I}_2$	$\text{m}^4 \text{W}^{-2} \text{s}^{-1}$
Out. Weight Mat.	\mathbf{Q}	$1 \cdot 10^{-4} \mathbf{I}_2$	$\text{K}^{-2} \text{s}^{-1}$
Imp. dist.	$\boldsymbol{\mu}(t) = \mathcal{N}(0, 100)$	⁴	$\text{kW}^2 \text{m}^{-4}$
Output dist.	$\boldsymbol{\nu}(t) = \mathcal{N}(0, 10)$	⁴	K^2
Init. Weight Mat.	\mathbf{S}	$1 \cdot 10^{-3} \mathbf{I}_5$	$\text{m}^2 \text{K}^{-2}$
Sim. Disc. Nodes	N_{fem}	41	

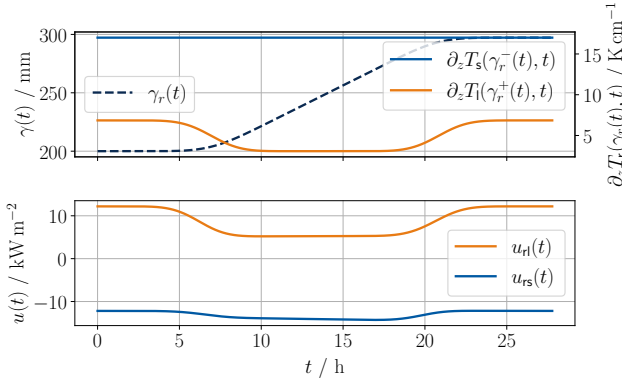
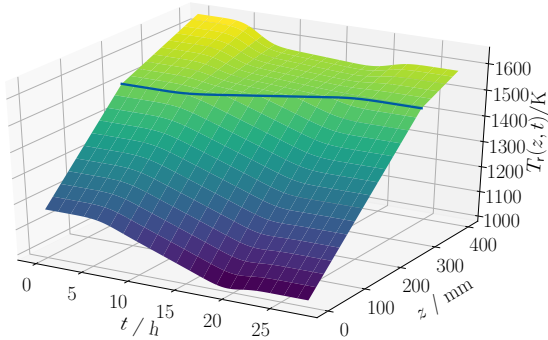


Figure 3: Reference trajectories for gradients and phase boundary (top) as well as the generated heater trajectories for the system inputs (bottom) of the feedforward control.


 Figure 4: Calculated reference temperature profile $T_r(z, t)$ with the reference phase boundary trajectory $\gamma_r(t)$ (blue).

of the distributed controller from Section 5 are analysed, using the standard (34) and modified tracking error (37).

As Figure 5a shows, the “fixed” collocated feedback (orange, solid) successfully corrects the initial error in the phase boundary position and tracks the reference. To do this however, a part of the already grown crystal has to be remolten which is to be avoided. In contrast, the collocated feedback with the shifted error system (orange, dashed) ignores the error in $\gamma(t)$ and makes no attempts on remelting the crystal. Furthermore, in Figure 5b it can be seen that this variant corrects the growth rate error faster than its fixed counterpart. However, a drawback that remains for this controller is that due to the simple reference shifting, a larger crystal is obtained at the end of the process if no further logic is superimposed.

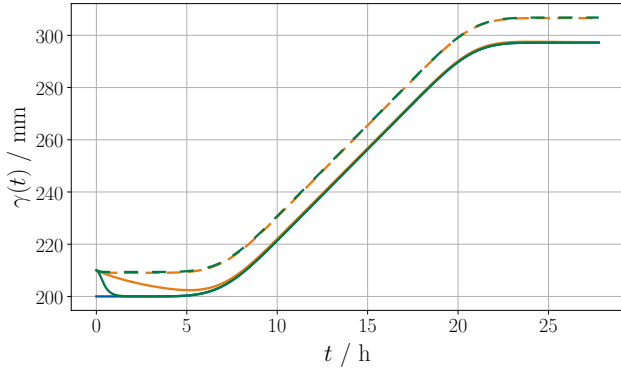
Now to the standard variant of the distributed feedback (green, solid). As it can be seen in Figure 5a, the error in $\gamma(t)$ is successfully corrected and the growth target is reached. Nevertheless, Figure 5b shows a severe spike in the growth rate, originating from the swift correction of $\gamma(t)$, thus remelting the crystal. Opposed to this, the version with the modified tracking error (green, dashed) tolerates the initial deviation in $\gamma(t)$ and continues tracking the trajectory of $\dot{\gamma}(t)$. However, as for the shifted variant of the collocated feedback, the deviation in $\gamma(t)$ still appears at the end. The control parameters for these simulations can be found in Appendix D.

7.3. Observer

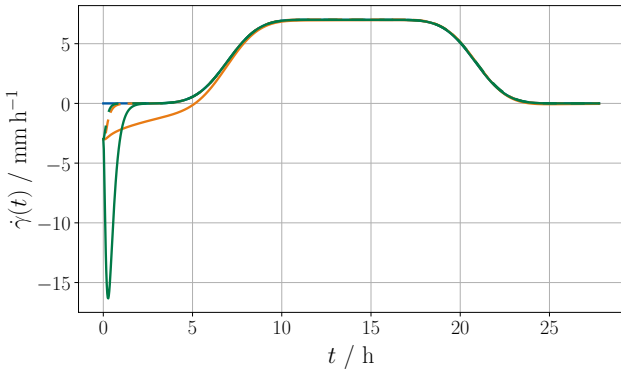
To analyse the observer performance a system under pure feedforward control is considered. For this case, the initial state estimate $\hat{\boldsymbol{\chi}}_N(0)$ of the observer is specified using the reference trajectory $\mathbf{y}_r(0)$. To examine the robustness against disturbances, the real system starts with the initial errors $\gamma_e(0) = 100 \text{ mm}$ and $\dot{\gamma}_e(0) = -3 \text{ mm h}^{-1}$ for both, the crystallisation interface and the growth rate, respectively. Furthermore, the process disturbances $\boldsymbol{\mu}(t)$ and $\boldsymbol{\nu}(t)$ are realised by zero-mean normal distributed noise, distorting the input and output measurements as illustrated in Figure 6. As Figure 7b displays, the state estimate quickly converges against the real one and the system state is properly tracked afterwards. Due to the different scales of the components in $\boldsymbol{\chi}^N(t)$, internally a scaled version $\tilde{\boldsymbol{\chi}}^N(t) = \mathcal{T}^N \boldsymbol{\chi}^N(t)$ has been used, with \mathcal{T}^N given in Appendix D.

7.4. Complete control system

To examine the performance of the feedback controller when supplied with the state estimates from the observer instead of the real system state, a similar setup is used. Particularly, the estimate is generated by an observer of type (39) which is using the model introduced in Subsection 5.1. By way of example, the distributed feedback controller with modified tracking error is used to close the control loop. As the bottom plot in Figure 8 shows, the closed loop performs as expected.



(a) Phase boundary position



(b) Growth velocity

Figure 5: Comparison of the tracking behaviour of the reference (blue) between collocated (orange) and distributed feedback (green) using the original (solid) or modified error (dashed), respectively. Note that the orange and green dashed lines are nearly equal.

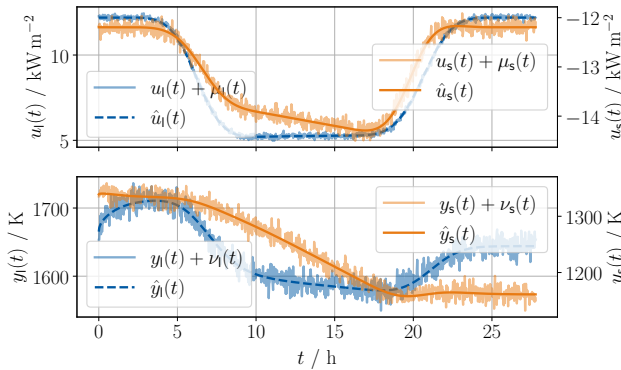


Figure 6: Inputs (top) and outputs (bottom) of the original system (dark) and their disturbed counterparts (light), used by the observer.

8. Conclusion and outlook

In this contribution, reference tracking control strategies for the VGF process, modelled as a two-phase SP have been presented. Based on the process demands not to remelt the already solidified domain, two different control approaches have been developed. The performance of components of the control system has been proven by a simulation study.

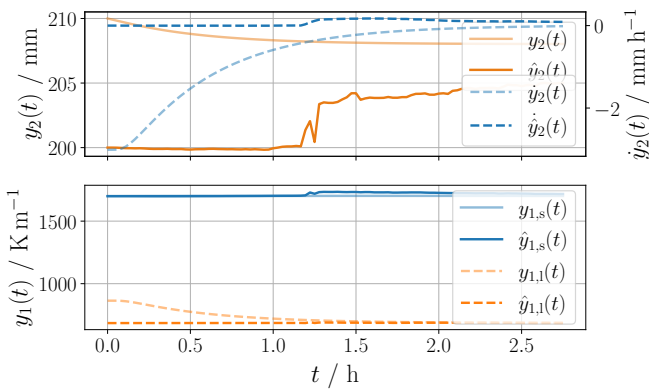
A drawback of the proposed solutions is the convergence of the utilised series for smaller transition times. While this is not a problem for the growth of GaAs, it may cause complications for the production of other materials. A direct alternative would be to use so called (N, ξ) -approximate k -sums as introduced in [30]. However, another promising approach is the control via a time-variant backstepping transformation c.f [31] which is currently under investigation and will be covered in a forthcoming publication.

Acknowledgments

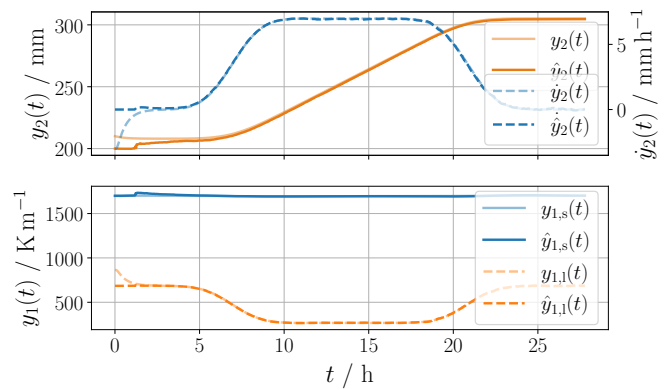
This work has been funded by the Deutsche Forschungsgemeinschaft (DFG) [project numbers WI 4412/1-1, FR 3671/1-1].

References

- [1] M. Jurisch, F. Börner, T. Bünger, S. Eichler, T. Flade, U. Kretzer, A. Köhler, J. Stenzenberger, B. Weinert, LEC- and VGF-growth of SI GaAs single crystals—recent developments and current issues, *Journal of Crystal Growth* 275 (1) (2005) 283 – 291, proceedings of the 14th International Conference on Crystal Growth and the 12th International Conference on Vapor Growth and Epitaxy. doi:10.1016/j.jcrysgro.2004.10.092.
- [2] J. Vanhellemont, The v/g criterion for defect-free silicon single crystal growth from a melt revisited: Implications for large diameter crystals, *Journal of Crystal Growth* 381 (2013) 134 – 138. doi:https://doi.org/10.1016/j.jcrysgro.2013.06.039.
- [3] C. Frank-Rotsch, N. Dropka, A. Glacki, U. Juda, VGF growth of GaAs utilizing heater-magnet module, *Journal of Crystal Growth* 401 (2014) 702–707.
- [4] N. Dropka, C. Frank-Rotsch, Accelerated VGF-crystal growth of GaAs under travelling magnetic fields, *Journal of Crystal Growth* 367 (2013) 1–7.
- [5] N. Dropka, C. Frank-Rotsch, Enhanced VGF-GaAs growth using pulsed unidirectional TMF, *Journal of Crystal Growth* 386 (2014) 146 – 153. doi:10.1016/j.jcrysgro.2013.09.027.
- [6] N. Dropka, C. Frank-Rotsch, GaAs — vertical gradient freeze process intensification, *Crystal Growth and Design* 14 (2014) 5122–5130.
- [7] P. Wellmann, G. Neubauer, L. Fahlbusch, M. Salamon, N. Uhlmann, Growth of SiC bulk crystals for application in power electronic devices – process design, 2D and 3D X-ray in situ visualization and advanced doping, *Cryst. Res. Technol.* 50 (2015) 2–9.
- [8] J. Crank, *Free and Moving Boundary Problems* (Oxford Science Publications), Oxford Science Publications, Oxford University Press, 1984.
- [9] S. Koga, M. Diagne, M. Krstic, Output feedback control of the one-phase Stefan problem, in: 2016 IEEE 55th Conference on Decision and Control (CDC), 2016, pp. 526–531. doi:10.1109/CDC.2016.7798322.



(a) Beginning



(b) Complete simulation

Figure 7: Estimates from the observer (dark), compared to the evolution of the real system's variables (light) for the phase boundary and growth rate (top) as well as the gradients at the phase boundary for crystal and melt.

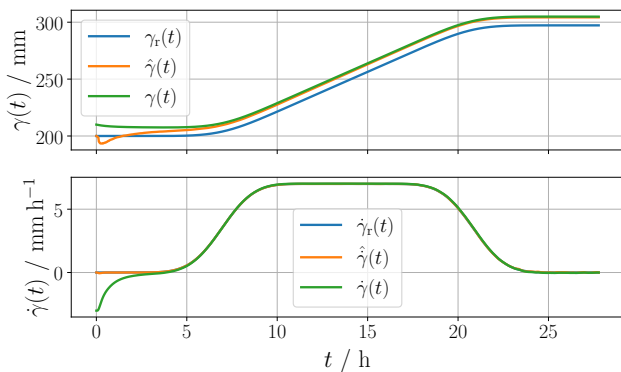


Figure 8: Resulting trajectories of the phase boundary (top) and the growth rate (bottom) for the complete control loop with distributed output feedback (green), compared to the reference (blue) and the estimated (orange).

[10] J. Brusche, A. Segal, C. Vuik, H. Urbach, A comparison of enthalpy and temperature methods for melting problems on composite domains, *Numerical Mathematics and Advanced Applications*.

[11] S. Chen, B. Merriman, S. Osher, P. Smereka, A simple level set method for solving Stefan problems, *Journal of Computational Physics*.

[12] G. Beckett, J. A. Mackenzie, M. L. Robertson, A moving mesh finite element method for the solution of two-dimensional Stefan problems, *Journal of Computational Physics* doi:10.1006/jcph.2001.6721.

[13] W. B. Dunbar, N. Petit, P. Rouchon, P. Martin, Motion planning for a nonlinear Stefan problem, *European Series in Applied and Industrial Mathematics (ESAIM): Control, Optimization and Calculus of Variations* 9 (2003) 275–296.

[14] B. Petrus, J. Bentsman, B. Thomas, Enthalpy-based feedback control algorithms for the Stefan problem, in: *Proceedings of the IEEE Conference on Decision and Control*, 2012, pp. 7037–7042.

[15] B. Petrus, J. Bentsman, B. G. Thomas, Application of enthalpy-based feedback control methodology to the two-sided stefan problem, in: *2014 American Control Conference*, 2014, pp. 1015–1020. doi:10.1109/ACC.2014.6859062.

[16] A. Maidi, J.-P. Corriou, Boundary geometric control of a linear

Stefan problem, *Journal of Process Control* 24 (6) (2014) 939 – 946, energy Efficient Buildings Special Issue. doi:https://doi.org/10.1016/j.jprocont.2014.04.010.

[17] S. Koga, M. Diagne, S. Tang, M. Krstic, Backstepping control of the one-phase Stefan problem, in: *2016 American Control Conference (ACC)*, 2016, pp. 2548–2553. doi:10.1109/ACC.2016.7525300.

[18] J. Rudolph, J. Winkler, F. Woittennek, Flatness based trajectory planning for two heat conduction problems in crystal growth technology, *e-STA (Sciences et Technologies de l'Automatique)* 1 (1).

[19] M. Hinze, O. Pätzold, S. Ziegenbalg, Solidification of a gas melt—optimal control of the phase interface, *Journal of Crystal Growth* 311 (8) (2009) 2501 – 2507. doi:https://doi.org/10.1016/j.jcrysgro.2009.02.031.

[20] B. Petrus, J. Bentsman, B. G. Thomas, Feedback control of the two-phase Stefan problem, with an application to the continuous casting of steel, in: *49th IEEE Conference on Decision and Control (CDC)*, 2010, pp. 1731–1736. doi:10.1109/CDC.2010.5717456.

[21] J. R. Cannon, *The One-Dimensional Heat Equation*, Vol. 23 of *Encyclopedia of Mathematics and its Applications*, Addison-Wesley, 1984.

[22] J. Stefan, Über die Theorie der Eisbildung, insbesondere über die Eisbildung in Polarmeere, *Annalen der Physikalischen Chemie* (1891) 269–286.

[23] J. Rudolph, J. Winkler, F. Woittennek, Flatness based control of distributed parameter systems: Examples and computer exercises from various technological domains, *Berichte aus der Steuerungs- und Regelungstechnik*, Shaker Verlag, Aachen, 2003.

[24] M. Gevrey, Sur la nature analytique des solutions des équations aux dérivées partielles. premier mémoire, *Annales scientifiques de l'École Normale Supérieure* 35 (1918) 129–190. URL <http://eudml.org/doc/81374>

[25] V. I. Zubov, *Methods of A.M. Lyapunov and their application*, P. Noordhoff, Groningen, 1964.

[26] A. Mironchenko, F. Wirth, A non-coercive Lyapunov framework for stability of distributed parameter systems, in: *2017 IEEE 56th Annual Conference on Decision and Control (CDC)*, 2017, pp. 1900–1905. doi:10.1109/CDC.2017.8263927.

[27] T. Meurer, Feedforward and feedback tracking control of diffusion-convection-reaction systems using summability methods, Ph.D. thesis, University of Stuttgart (2005). doi:http://dx.doi.org/10.18419/opus-4075.

[28] T. Meurer, M. Zeitz, Feedforward and feedback tracking control of nonlinear diffusion-convection-reaction systems using summability methods, *Industrial & Engineering Chemistry Re-*

search 44 (8) (2005) 2532–2548. arXiv:<https://doi.org/10.1021/ie0495729>, doi:10.1021/ie0495729.

URL <https://doi.org/10.1021/ie0495729>

- [29] E. D. Sontag, *Mathematical Control Theory*, 2nd Edition, Vol. 6 of Texts in Applied Mathematics, Springer-Verlag, 1998.
- [30] T. Meurer, M. Zeitz, Flatness-based feedback control of diffusion-convection-reaction systems via k-summable power series, *IFAC Proceedings Volumes* 37 (13) (2004) 177 – 182, 6th IFAC Symposium on Nonlinear Control Systems 2004 (NOLCOS 2004), Stuttgart, Germany, 1-3 September, 2004. doi: [https://doi.org/10.1016/S1474-6670\(17\)31219-3](https://doi.org/10.1016/S1474-6670(17)31219-3).
- [31] T. Meurer, A. Kugi, Tracking control for boundary controlled parabolic pdes with varying parameters: Combining backstepping and differential flatness, *Automatica* 45 (5) (2009) 1182 – 1194. doi:<https://doi.org/10.1016/j.automatica.2009.01.006>.
URL <http://www.sciencedirect.com/science/article/pii/S0005109809000478>
- [32] A. S. Miroslav Krstic, *Boundary control of PDEs: a course on backstepping designs*, siam Edition, *Advances in Design and Control*, Society for Industrial and Applied Mathematic, 2008.

Appendix A. Transformations

Appendix A.1. Moving reference system

The coordinate transform

$$\tilde{T}(\tilde{z}, t) = T(z, t) \quad \text{with} \quad \tilde{z} := z - \gamma(t)$$

Taking the partial derivative w.r.t. z gives

$$\partial_z^2 T(z, t) = \partial_{\tilde{z}}^2 \tilde{T}(\tilde{z}, t) \quad (\text{A.1})$$

while according to the chain rule, the time derivative becomes

$$\begin{aligned} \partial_t T(z, t) &= \frac{d}{dt} \left(\tilde{T}(\tilde{z}, t) \right) = \partial_{\tilde{z}} \tilde{T}(\tilde{z}, t) \partial_t \tilde{z}(t) + \partial_t \tilde{T}(\tilde{z}, t) \\ &= -\partial_{\tilde{z}} \tilde{T}(\tilde{z}, t) \dot{\gamma}(t) + \partial_t \tilde{T}(\tilde{z}, t) \end{aligned} \quad (\text{A.2})$$

where $\dot{\gamma}(t)$ denotes the growth rate. Inserting (A.2) and (A.1) into (2) yields the transformed generic system

$$\begin{aligned} \partial_t \tilde{T}(\tilde{z}, t) &= \alpha_o \partial_{\tilde{z}}^2 \tilde{T}(\tilde{z}, t) + \dot{\gamma}(t) \partial_{\tilde{z}} \tilde{T}(\tilde{z}, t) \\ k_o \partial_{\tilde{z}} \tilde{T}(\Gamma_o - \tilde{z}, t) &= \delta u_o(t) \\ \tilde{T}(0, t) &= T_m. \end{aligned}$$

Appendix A.2. Shifted error system

The evolution of the “shifted” error can be described by taking the time derivative of (19) for the real and the planned profile

$$\begin{aligned} \partial_t \tilde{e}(z, t) &= \partial_t T(z, t) - \frac{d}{dt} (T_r(z - \Delta\gamma(t), t)) \\ &= \partial_t T(z, t) - \partial_t T_r(z - \Delta\gamma(t), t) \\ &\quad + \partial_z T_r(z - \Delta\gamma(t), t) \Delta\dot{\gamma}(t) \end{aligned}$$

and then substituting the partial differential equations (PDEs) according to (2), which hold for the real as well as for the reference system:

$$\begin{aligned} \partial_t \tilde{e}(z, t) &= \alpha_o \partial_z^2 T(z, t) - \alpha_o \partial_z^2 T_r(z - \Delta\gamma(t), t) \\ &\quad + \Delta\dot{\gamma}(t) \partial_z T_r(z - \Delta\gamma(t), t). \end{aligned}$$

Making use of definition (19), one arrives at

$$\partial_t \tilde{e}(z, t) = \alpha_o \partial_z^2 \tilde{e}(z, t) + \Delta\dot{\gamma}(t) \partial_z T_r(z - \Delta\gamma(t), t),$$

while the related boundary conditions are given by

$$\begin{aligned} \partial_z \tilde{e}(\Gamma_o, t) &= \partial_z T(\Gamma_o, t) - \partial_z T_r(\Gamma_o - \Delta\gamma(t), t) \\ &= \frac{\delta}{k_o} u(t) - \partial_z T_r(\Gamma_o - \Delta\gamma(t)) \\ \tilde{e}(\gamma(t), t) &= T(\gamma(t), t) - T_r(\gamma(t) - \Delta\gamma(t), t) \\ &= T_m - T_m = 0. \end{aligned}$$

Hence, the resulting error system is governed by

$$\begin{aligned} \partial_t \tilde{e}(z, t) &= \alpha_o \partial_z^2 \tilde{e}(z, t) + \Delta\dot{\gamma}(t) \partial_z T_r(z - \Delta\gamma(t), t) \\ \partial_z \tilde{e}(\Gamma_o, t) &= \frac{\delta}{k_o} u(t) - \partial_z T_r(\Gamma_o - \Delta\gamma(t), t) \\ \tilde{e}(\gamma(t), t) &= 0. \end{aligned}$$

Appendix B. Stability analysis

Firstly, $V(\boldsymbol{\xi})$ is decomposed into

$$V(\boldsymbol{\xi}) = V_s(\boldsymbol{\xi}) + V_1(\boldsymbol{\xi}) \quad (\text{B.1})$$

with $V_s(\boldsymbol{\xi}) = \frac{1}{2} \int_{\Gamma_s}^{\gamma(t)} \tilde{e}_s^2(z, t) dz$ and $V_1(\boldsymbol{\xi}) = \frac{1}{2} \int_{\gamma(t)}^{\Gamma_1} \tilde{e}_1^2(z, t) dz$.

For the sake of brevity, the next steps will focus on the generic function $V_o(\boldsymbol{\xi})$ since they are similar for $V_s(\boldsymbol{\xi})$ and $V_1(\boldsymbol{\xi})$. Differentiation of

$$V_o(\boldsymbol{\xi}) = \frac{\delta_o}{2} \int_{\gamma(t)}^{\Gamma_o} \tilde{e}_o^2(z, t) dz \quad (\text{B.2})$$

leads to

$$\dot{V}_o(\boldsymbol{\xi}) = -\frac{\delta_o}{2} \dot{\gamma}(t) \tilde{e}_o^2(\gamma(t), t) + \delta_o \int_{\gamma(t)}^{\Gamma_o} \tilde{e}_o(z, t) \partial_t \tilde{e}_o(z, t) dz.$$

Using (20c) and substituting the system dynamics (20a) one obtains

$$\begin{aligned} \dot{V}_o(\boldsymbol{\xi}) &= \delta_o \int_{\gamma(t)}^{\Gamma_o} \tilde{e}_o(z, t) \left(\alpha_o \partial_z^2 \tilde{e}(z, t) \right. \\ &\quad \left. + \Delta\dot{\gamma}(t) \partial_z T_{o,r}(z - \Delta\gamma(t), t) \right) dz. \end{aligned}$$

Integration by parts of the first summand yields

$$\begin{aligned} \dot{V}_o(\boldsymbol{\xi}) &= \alpha_o \delta_o \left[\tilde{e}_o(z, t) \partial_z \tilde{e}_o(z, t) \right]_{\gamma(t)}^{\Gamma_s} \\ &\quad - \alpha_o \delta_o \int_{\gamma(t)}^{\Gamma_s} (\partial_z \tilde{e}_o(z, t))^2 dz \\ &\quad + \delta_o \Delta\dot{\gamma}(t) \int_{\gamma(t)}^{\Gamma_s} \tilde{e}_o(z, t) \partial_z T_{o,r}(z - \Delta\gamma(t), t) dz. \end{aligned}$$

Using the boundary conditions (20b), (20c) as well as the feedback law (23) gives

$$\begin{aligned} &= -\alpha_o \kappa_o \tilde{e}_o^2(\Gamma_o, t) - \alpha_o \delta_o \int_{\gamma(t)}^{\Gamma_o} (\partial_z \tilde{e}_o)^2 dz \\ &+ \delta_o \Delta \dot{\gamma}(t) \int_{\gamma(t)}^{\Gamma_o} \tilde{e}_o \partial_z T_{o,r}(z - \Delta \gamma(t), t) dz \end{aligned} \quad (\text{B.3})$$

since $\delta_o^2 = 1$. To reassemble $\dot{V}_o(\boldsymbol{\xi})$ in the expression, the first term has to be rearranged. Therefore, a slightly modified version of the Poincaré inequality (CSI) is introduced, based on the one given in [32].

Poincaré inequality. Consider the partially integrated term

$$\begin{aligned} \int_{\gamma(t)}^{\Gamma_o} \tilde{e}_o^2(z, t) dz &= [z \tilde{e}_o^2(z, t)]_{\gamma(t)}^{\Gamma_o} - 2 \int_{\gamma(t)}^{\Gamma_o} z \tilde{e}_o(z, t) \partial_z \tilde{e}_o(z, t) dz \\ &= \Gamma_o \tilde{e}_o^2(\Gamma_o, t) - 2 \int_{\gamma(t)}^{\Gamma_o} z \tilde{e}_o(z, t) \partial_z \tilde{e}_o(z, t) dz \end{aligned}$$

which, by making use of the Cauchy-Schwarz inequality (CSI), can be estimated as

$$\int_{\gamma(t)}^{\Gamma_o} \tilde{e}_o^2(z, t) dz \leq \overbrace{\sqrt{\int_{\gamma(t)}^{\Gamma_o} \tilde{e}_o^2(z, t) dz}}{=:a} \overbrace{2 \sqrt{\int_{\gamma(t)}^{\Gamma_o} (z \partial_z \tilde{e}_o(z, t))^2 dz}}{=:b} + \Gamma_o \tilde{e}_o^2(\Gamma_o, t).$$

Using Young's inequality (YI) $ab \leq \frac{1}{2\sigma} a^2 + \frac{\sigma}{2} b^2$ with $\sigma = 1$ one arrives at

$$\int_{\gamma(t)}^{\Gamma_o} \tilde{e}_o^2(z, t) dz \leq \frac{1}{2} \int_{\gamma(t)}^{\Gamma_o} \tilde{e}_o^2(z, t) dz + 2 \int_{\gamma(t)}^{\Gamma_o} (z \partial_z \tilde{e}_o(z, t))^2 dz + \Gamma_o \tilde{e}_o^2(\Gamma_o, t),$$

which after rearranging can be further estimated by

$$\begin{aligned} \frac{1}{2} \int_{\gamma(t)}^{\Gamma_o} \tilde{e}_o(z, t) dz &\leq 2 \int_{\gamma(t)}^{\Gamma_o} (z \partial_z \tilde{e}_o(z, t))^2 dz + \Gamma_o \tilde{e}_o^2(\Gamma_o, t) \\ &\leq 2\Gamma_1^2 \int_{\gamma(t)}^{\Gamma_o} (\partial_z \tilde{e}_o(z, t))^2 dz + \Gamma_o \tilde{e}_o^2(\Gamma_o, t), \end{aligned}$$

since $\Gamma_s \leq \gamma(t) \leq \Gamma_1 \forall t$. Further rearrangement finally provides the required inequality:

$$- \int_{\gamma(t)}^{\Gamma_o} (\partial_z \tilde{e}_o(z, t))^2 dz \leq -\frac{1}{4\Gamma_1^2} \int_{\gamma(t)}^{\Gamma_o} \tilde{e}_o^2(z, t) dz - \frac{\Gamma_o}{2\Gamma_1^2} \tilde{e}_o^2(\Gamma_o, t). \quad (\text{B.4})$$

Reassembly. Substitution of (B.4) in (B.3) yields

$$\begin{aligned} \dot{V}_o(\boldsymbol{\xi}) &\leq -\alpha_o \tilde{e}_o^2(\Gamma_o, t) \left(\kappa_o + \frac{\delta_o \Gamma_o}{2\Gamma_1^2} \right) - \frac{\alpha_o \delta_o}{4\Gamma_1^2} \int_{\gamma(t)}^{\Gamma_o} \tilde{e}_o^2(z, t) dz \\ &+ \delta_o \Delta \dot{\gamma}(t) \int_{\gamma(t)}^{\Gamma_o} \tilde{e}_o(z, t) \partial_z T_{o,r}(z - \Delta \gamma(t), t) dz. \end{aligned}$$

Thus, comparison with (B.2) leads to

$$\begin{aligned} &\leq -b_o \tilde{e}_o^2(\Gamma_o, t) - \frac{\alpha_o}{2\Gamma_1^2} V_o(\boldsymbol{\xi}) \\ &+ \Delta \dot{\gamma}(t) \int_{\gamma(t)}^{\Gamma_o} \tilde{e}_o(z, t) \partial_z T_{o,r}(z - \Delta \gamma(t), t) dz \end{aligned}$$

with the positive constant $b_o = \alpha_o \left(\kappa_o + \frac{\delta_o \Gamma_o}{2\Gamma_1^2} \right)$ by an appropriate choice of κ_o . Hence, by substituting the results for $V_s(\boldsymbol{\xi})$ and $V_1(\boldsymbol{\xi})$ in (B.1), $\dot{V}(\boldsymbol{\xi})$ can be expressed as

$$\begin{aligned} \dot{V}(\boldsymbol{\xi}) &\leq -b_s \tilde{e}_s^2(\Gamma_s, t) - b_1 \tilde{e}_1^2(\Gamma_1, t) - CV(\boldsymbol{\xi}) \\ &+ \Delta \dot{\gamma}(t) \int_{\Gamma_s}^{\Gamma_1} \tilde{e}(z, t) \partial_z T_r(z - \Delta \gamma(t), t) dz \end{aligned} \quad (\text{B.5})$$

with $C = \frac{1}{2\Gamma_1^2} \max\{\alpha_s, \alpha_1\} \geq 0$.

Simplified variant. Choosing the reference profile to be constant w.r.t. the spatial dimension z makes the integral term in (B.5) vanish. This can be achieved by using the reference $T_r^0 \equiv T_m$, which may be the case if the process should be brought to halt. The resulting derivative

$$\dot{V}(\boldsymbol{\xi}) \leq -b_s \tilde{e}_s^2(\Gamma_s, t) - b_1 \tilde{e}_1^2(\Gamma_1, t) - CV(\boldsymbol{\xi}) \quad (\text{B.6})$$

is obviously negative definite, yielding uniformly, globally, asymptotic stability of the system (20a) with respect to \mathcal{A} for this case.

General variant. Ignoring the boundary terms in (B.5) and focussing on the last term, by using CSI, the estimation

$$\Delta \dot{\gamma}(t) \int_{\Gamma_s}^{\Gamma_1} \tilde{e}(z, t) \partial_z T_r(z - \Delta \gamma(t), t) dz \leq |\Delta \dot{\gamma}(t)| K \sqrt{V(\boldsymbol{\xi})}$$

is obtained, where $K = \sqrt{2}(\Gamma_1 - \Gamma_s) \max_{z,t} |\partial_z T_r(z, t)|$. Summarizing, $\dot{V}(\boldsymbol{\xi})$ is bounded by

$$\dot{V}(\boldsymbol{\xi}) \leq -CV(\boldsymbol{\xi}) + |\Delta \dot{\gamma}(t)| K \sqrt{V(\boldsymbol{\xi})}. \quad (\text{B.7})$$

Furthermore, for every $V(\boldsymbol{\xi})$ a scaling $\nu > 0$ can be found such that

$$V(\boldsymbol{\xi}) \geq \nu \sqrt{V(\boldsymbol{\xi})}$$

holds. As a consequence, for $V(\boldsymbol{\xi}) \geq \nu^2$ the estimate

$$\dot{V}(\boldsymbol{\xi}) \leq (|\Delta\dot{\gamma}(t)| \bar{K} - C) V(\boldsymbol{\xi}) \quad (\text{B.8})$$

with $\bar{K} = \frac{K}{\nu}$ can be used. Finally by using Gronwall's lemma, a growth bound for $V(\boldsymbol{\xi})$ is given by

$$V(\boldsymbol{\xi}) \leq V(0) \exp(\bar{K} \Psi_0^t(\Delta\gamma) - Ct). \quad (\text{B.9})$$

Thus, (26) is decreasing for $V(\boldsymbol{\xi}) \geq \nu^2$ if

$$\Psi_0^t(\Delta\gamma) \leq \frac{C}{\bar{K}} t \quad (\text{B.10})$$

holds, hence, if there exists an upper bound for the total variation $\Psi_0^t(\Delta\gamma)$ that grows linear in time.

Appendix C. Matrices and Vectors

$$\begin{aligned} \mathbf{P}_{0,0} &= \begin{pmatrix} \langle \bar{\varphi}_0(\bar{z}) | \bar{\varphi}_0(\bar{z}) \rangle & \dots & \langle \bar{\varphi}_{N-1}(\bar{z}) | \bar{\varphi}_0(\bar{z}) \rangle \\ \vdots & \ddots & \vdots \\ \langle \bar{\varphi}_0(\bar{z}) | \bar{\varphi}_{N-1}(\bar{z}) \rangle & \dots & \langle \bar{\varphi}_{N-1}(\bar{z}) | \bar{\varphi}_{N-1}(\bar{z}) \rangle \end{pmatrix} \\ \mathbf{P}_{1,0} &= \begin{pmatrix} \langle \bar{z} \partial_{\bar{z}} \bar{\varphi}_0(\bar{z}) | \bar{\varphi}_0(\bar{z}) \rangle & \dots & \langle \bar{z} \partial_{\bar{z}} \bar{\varphi}_{N-1}(\bar{z}) | \bar{\varphi}_0(\bar{z}) \rangle \\ \vdots & \ddots & \vdots \\ \langle \bar{z} \partial_{\bar{z}} \bar{\varphi}_0(\bar{z}) | \bar{\varphi}_{N-1}(\bar{z}) \rangle & \dots & \langle \bar{z} \partial_{\bar{z}} \bar{\varphi}_{N-1}(\bar{z}) | \bar{\varphi}_{N-1}(\bar{z}) \rangle \end{pmatrix} \\ \mathbf{P}_{1,1} &= \begin{pmatrix} \langle \partial_{\bar{z}} \bar{\varphi}_0(\bar{z}) | \bar{\varphi}_0(\bar{z}) \rangle & \dots & \langle \partial_{\bar{z}} \bar{\varphi}_{N-1}(\bar{z}) | \bar{\varphi}_0(\bar{z}) \rangle \\ \vdots & \ddots & \vdots \\ \langle \partial_{\bar{z}} \bar{\varphi}_0(\bar{z}) | \bar{\varphi}_{N-1}(\bar{z}) \rangle & \dots & \langle \partial_{\bar{z}} \bar{\varphi}_{N-1}(\bar{z}) | \bar{\varphi}_{N-1}(\bar{z}) \rangle \end{pmatrix} \\ \mathbf{q}_{1,0} &= \begin{pmatrix} \langle \bar{z} \partial_{\bar{z}} \bar{\varphi}_N(\bar{z}) | \bar{\varphi}_0(\bar{z}) \rangle \\ \vdots \\ \langle \bar{z} \partial_{\bar{z}} \bar{\varphi}_N(\bar{z}) | \bar{\varphi}_{N-1}(\bar{z}) \rangle \end{pmatrix}, \mathbf{q}_{1,1} = \begin{pmatrix} \langle \partial_{\bar{z}} \bar{\varphi}_N(\bar{z}) | \bar{\varphi}_0(\bar{z}) \rangle \\ \vdots \\ \langle \partial_{\bar{z}} \bar{\varphi}_N(\bar{z}) | \bar{\varphi}_{N-1}(\bar{z}) \rangle \end{pmatrix} \end{aligned}$$

Appendix D. Control parameters

The parameters of the collocated feedback have been chosen as $\kappa_s = \kappa_l = 20 \text{ m}^{-1}$, while the distributed feedback was parametrised with $\kappa_{1,0} = 2 \cdot 10^{-6} \text{ m}^{-2}$, $\kappa_{1,1} = 3 \cdot 10^{-3} \text{ m}^{-1}$ as well as $\kappa_{2,0} = 6 \cdot 10^{-9} \text{ s}^{-3}$, $\kappa_{2,1} = 1.1 \cdot 10^{-5} \text{ s}^{-2}$, $\kappa_{2,2} = 6 \cdot 10^{-3} \text{ s}^{-1}$ for the original and $\tilde{\kappa}_{2,0} = 6 \cdot 10^{-6} \text{ s}^{-2}$, $\tilde{\kappa}_{2,1} = 5 \cdot 10^{-3} \text{ s}^{-1}$ for the modified error.

The scaling matrix for $\tilde{\chi}^5(t)$ was chosen as

$$\mathcal{T}^5 = \text{diag}(1 \cdot 10^{-3}, 1 \cdot 10^{-3} \text{ m}, 1 \cdot 10^7, 1 \cdot 10^{10} \text{ m}, 1 \cdot 10^{13} \text{ m}^2).$$